Title
Splicing Activation by Rbfox Requires Self-Aggregation through Its Tyrosine-Rich Domain

Journal
Cell, 170(2)

ISSN
0092-8674

Authors
Ying, Yi
Wang, Xiao-Jun
Vuong, Celine K
et al.

Publication Date
2017-07-01

DOI
10.1016/j.cell.2017.06.022

Peer reviewed

HHS Public Access

Author manuscript

Cell. Author manuscript; available in PMC 2018 July 13.

Published in final edited form as:

Cell. 2017 July 13; 170(2): 312–323.e10. doi:10.1016/j.cell.2017.06.022.

Splicing activation by Rbfox requires self-aggregation through its tyrosine-rich domain

Yi Ying[1,3], **Xiao-Jun Wang**[2], **Celine K. Vuong**[1,3], **Chia-Ho Lin**[2], **Andrey Damianov**[2], and **Douglas L. Black**[2,3,4,*]

[1]Molecular Biology Interdepartmental Doctoral Program

[2]Department of Microbiology, Immunology, and Molecular Genetics

[3]Molecular Biology Institute, University of California, Los Angeles, Los Angeles, CA 90095, USA

SUMMARY

Proteins of the Rbfox family act with a complex of proteins called the Large Assembly of Splicing Regulators, LASR. We find that Rbfox interacts with LASR via its C-terminal domain (CTD) and this domain is essential for its splicing activity. In addition to LASR recruitment, a low complexity (LC) sequence within the CTD contains repeated tyrosines that mediate higher-order assembly of Rbfox/LASR and are required for splicing activation by Rbfox. This sequence spontaneously aggregates in solution to form fibrous structures and hydrogels, suggesting an assembly similar to the insoluble cellular inclusions formed by FUS and other proteins in neurologic disease. Unlike the pathological aggregates, we find that assembly of the Rbfox CTD plays an essential role in its normal splicing function. Rather than simple recruitment of individual regulators to a target exon, alternative splicing choices also depend on the higher-order assembly of these regulators within the nucleus.

Graphical abstract

[*]Correspondence: dougb@microbio.ucla.edu.
[4]Lead Contact

AUTHOR CONTRIBUTIONS

Conceptualization, Y.Y. and D.L.B.; Methodology, Y.Y., X.-J.W., C.K.V., A.D., and D.L.B.; Investigation, Y.Y., X.-J.W., C.K.V., and A.D.; Formal Analysis, Y.Y. and C.-H.L.; Data Curation, Y.Y. and C.-H.L.; Writing – Original Draft, Y.Y. and D.L.B.; Writing – Review and Editing, Y.Y., X.-J.W., C.K.V., C.-H.L., A.D., and D.L.B.; Supervision, D.L.B.; Project Administration, D.L.B.; Funding Acquisition, D.L.B.

Data and Software Availability

The RASL-seq data has been deposited to the NCBI GEO under the accession number GSE89597.

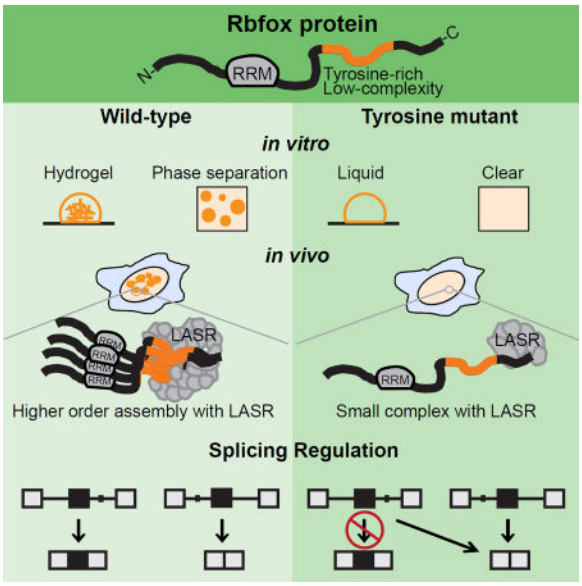

INTRODUCTION

RNA-binding proteins (RBPs) control all aspects of RNA metabolism from biogenesis to decay (Singh et al., 2015). These proteins contain various classes of RNA-binding domains (RBDs) that recognize a wide range of short RNA elements, as well as auxiliary non-RNA binding domains that often contain intrinsically disordered regions (IDR) and sequences of low amino acid complexity (LC) (Calabretta and Richard, 2015). Recent studies have found that certain IDR and LC domains can form fibers or phase-separated liquid droplets *in vitro* (Courchaine et al., 2016; Lin et al., 2015; Molliex et al., 2015; Nott et al., 2015; Schwartz et al., 2015). These sequences can further condense into highly stable hydrogel assemblies containing an amyloid-like cross-beta structure (Eisenberg and Jucker, 2012; Kato et al., 2012; Murakami et al., 2015; Patel et al., 2015). Considerable interest in these aggregation properties stems from the discovery that RNA-binding proteins such as FUS and TDP-43 form stable amyloid-like cellular inclusions in Amyotrophic Lateral Sclerosis (ALS) and other neurological pathologies (Lagier-Tourenne and Cleveland, 2009). Recent work has also found that IDR or LC sequences function in normal cytoplasmic mRNA metabolism to allow the reversible concentration of RBPs within membrane-free subcellular organelles such as stress granules or RNP granules (Courchaine et al., 2016; Jain et al., 2016; Kato et al., 2012; Kroschwald et al., 2015; Wallace et al., 2015). The nuclear RBPs involved in splicing also have extensive LC sequences, but roles for these sequences and their aggregation are not yet defined.

The regulation of alternative pre-mRNA splicing involves a very large number of RBPs that bind nascent transcripts to alter spliceosome assembly and splice site choice (Fu and Ares, 2014; Lee and Rio, 2015). One family of splicing regulators is the Rbfox proteins that control networks of spliced isoform expression in brain, heart and muscle, and during embryonic development (Conboy, 2017). There are three mammalian Rbfox genes (Rbfox1, Rbfox2, and Rbfox3) each with a single RNA recognition motif (RRM) that binds the short

element (U)GCAUG (Auweter et al., 2006). Alternative promoters and alternative splicing diversify the products of each gene, generating both nuclear and cytoplasmic isoforms (Damianov and Black, 2010; Lee et al., 2009; Nakahata and Kawamoto, 2005). The N and C terminal domains have segments of low amino acid complexity and undefined structure whose function is unknown (Figure S1A and data not shown).

Clinical interest in the Rbfox proteins stems from findings that RBFOX1 can be mutated in patients with autism spectrum disorders and epilepsy (Bill et al., 2013; Lal et al., 2013). Similarly, homozygous null Rbfox1 mutations in the mouse brain lead to a seizure phenotype (Gehman et al., 2011). Changes in Rbfox1 expression, and in the splicing and expression of Rbfox1 target transcripts, were also observed in brains of ASD patients (Lee et al., 2016; Parikshak et al., 2016; Voineagu et al., 2011; Weyn-Vanhentenryck et al., 2014).

Recently we showed that Rbfox proteins regulate splicing while bound with the Large Assembly of Splicing Regulators, LASR, a multiprotein complex of eight RNA-binding proteins (Damianov et al., 2016). Rbfox/LASR complexes sedimented at ~55S on density gradients, indicating assemblies larger than a single Rbfox bound to a single LASR, but the nature and significance of the interactions leading to this higher-order assembly were unresolved. Here we report that the C-terminal domain (CTD) of Rbfox interacts with LASR and is required for splicing regulation. An LC sequence within the CTD mediates higher-order assembly of Rbfox/LASR and nuclear speckle localization *in vivo*, as well as formation of fibrous aggregates and hydrogels *in vitro*. Mutations that block the higher-order assembly of Rbfox but not its LASR interaction prevent proper splicing regulation and establish a link between the biophysical properties of Rbfox aggregation and its function in splicing.

RESULTS

The C-terminal domain (CTD) of Rbfox mediates interaction with LASR and higher-order assembly

To identify regions of Rbfox1 responsible for interacting with LASR, we generated Flp-In T-REx 293 cell lines stably expressing deletion mutants of Rbfox1 tagged with the HA-FLAG epitopes and the SV40 NLS (Figure 1A). We isolated Rbfox/LASR complexes from these cells by FLAG immunoprecipitation and peptide elution, as previously described (Damianov et al., 2016). The complete set of LASR proteins was co-immunoprecipitated with Rbfox missing either the N-terminal domain (NTD) or the RNA-binding domain (RBD), indicating that these two regions are not essential for interaction with LASR (Figure 1B). Although all LASR components were present in these samples, some subunits, such as hnRNP UL2, were isolated in lower amounts, suggesting that the NTD and RBD may provide additional contacts for particular proteins. In contrast, deletion of the CTD (ΔCTD) abolished the interaction with LASR, and the CTD fragment alone co-immunoprecipitated the LASR subunits with similar efficiency to full-length Rbfox1 (Figure 1B). Thus the CTD provides the primary contact with LASR.

We previously found that Rbfox1 sediments in glycerol gradients as a larger assembly than predicted for a single Rbfox/LASR complex (Damianov et al., 2016). Examining the mutant

proteins, we found that the CTD fragment sedimented as a higher-order complex of approximately 55S similar to the full-length protein, while ΔCTD remained at the top of the glycerol gradient (Figure 1C). These results demonstrate that the Rbfox CTD is necessary and sufficient both to interact with LASR and to form higher-order complexes.

Repetitive tyrosine residues within the CTD are essential for higher-order assembly of Rbfox1

Rbfox1, Rbfox2, and Rbfox3 paralogs all form the higher-order complexes seen in gradients. These were observed both with the endogenous proteins in mouse brain and with ectopically expressed proteins in HEK293 cells (Damianov et al., 2016). Rbfox1 and Rbfox2 also have muscle-specific variants derived from the inclusion of exon M43 instead of exon B40 (Damianov and Black, 2010). Exons M43 and B40 encode related but not identical amino acid sequences within the CTD (Figure 1D). Examining the M43 variants on glycerol gradients, we found that Rbfox1_M43 peaked in the 55S region similar to Rbfox1_B40 and Rbfox2_B40. Strikingly, Rbfox2_M43 did not form higher-order complexes, but instead sedimented as a much smaller species near the top of the gradient (Figure 1D). The difference in sedimentation is attributed to the M43 segment, as a hybrid Rbfox1 protein containing the M43 exon of Rbfox2 (Rbfox1_2M43) also largely sedimented as small complexes (Figure 1D). These data suggest that Rbfox2_M43 might lack residues needed for the higher-order assembly. Aligning the exon sequences, it was notable that of three tyrosine residues in the B40 exons, two were conserved in Rbfox1_M43 but all were missing from Rbfox2_M43 (Figure 1D).

Looking at the CTD region, we found additional tyrosine residues upstream and particularly downstream of exon B40, with the downstream residues more closely spaced (Figure 1E). To examine the role of these tyrosines, we created a series of mutant Rbfox1 proteins with increasing numbers of tyrosines changed to serines or alanines. An Rbfox1 mutant with the three tyrosine residues of exon B40 replaced by serine or alanine sedimented only partially at 55S, with a substantial fraction of the protein shifted to near the top of the gradient (Figure 1F, changing tyrosines 1–3 in Figure 1E). Mutation of additional tyrosines nearly eliminated higher-order assembly (Figure 1F, changing tyrosines 1–6, 1–7, or 1–10 in Figure 1E). Serine substitutions showed a slightly stronger effect than alanine. In contrast, changing three tyrosines to phenylalanines did not impair the higher-order assembly of Rbfox1, suggesting that aromatic interactions contribute to the assembly (Figure 1F).

Given that the CTD was required for the Rbfox interaction with LASR, it was possible that the higher-order assembly involved interactions of LASR proteins and that the effect of the tyrosine mutations reflected a loss of LASR binding to Rbfox. This proved not to be the case. All the tyrosine-to-serine mutants as well as Rbfox2_M43 retain their interaction with LASR, immunoprecipitating LASR with equal efficiency to wild type protein (Figure 1G and data not shown). The property of higher-order assembly by Rbfox is apparently separate from the LASR interaction.

To further define the interactions between Rbfox and LASR, we divided the CTD region into three fragments, C1, C2, and C3 (Figure 1E). C1 included the sequence upstream of the ten mutated tyrosines. C2 contained exon B40 and all 10 of the mutated tyrosines. C3 contained

the extreme C-terminus including some additional tyrosines and the NLS. Each of these C-terminal regions was fused to the Rbfox1 ΔCTD protein, which did not interact with LASR on its own (Figure 1B). Adding C1 to Rbfox1 ΔCTD had little effect, with the protein pulling down only small amounts of LASR (Figure 2A, bottom), and not forming higher-order complexes (Figure 2B). In contrast, Rbfox1 ΔCTD fused to either C2 or C3 pulled down LASR relatively efficiently (Figure 2A, bottom). C2 was more prone to aggregation into higher-order complexes than C3 (Figure 2B). The medium-size complexes in fractions 7 to 9 formed by C3 may result from tyrosines not tested by mutation. Mutation of the tyrosines in C2 to serines eliminated the higher-order assembly, and unlike the full length protein also reduced the interaction with LASR (Figure 2). These data indicate that subregions of the CTD can independently bind LASR and that in some segments the tyrosines contribute to this interaction.

Aggregation of the CTD alone

A variety of aggregation properties have been reported for the LC sequences of RNA-binding proteins, including the formation of hydrogels, amyloid-like fibrils, and phase-separated liquid droplets (Aguzzi and Altmeyer, 2016; Bergeron-Sandoval et al., 2016; Kato et al., 2012; Lin et al., 2015). The LC sequence of the FUS protein contains the repeated tripeptide [G/S]Y[G/S] that mediates its assembly into an amyloid-like cross-beta structure (Kato et al., 2012). Although not exact matches to the FUS tripeptide motif, many of the tyrosines in the Rbfox1 C2 region are preceded or followed by glycine or serine. We found that polypeptides of the CTD were predicted as potential hot spots of amyloidal aggregation by AGGRESCAN (Conchillo-Sole et al., 2007) (Figure S1A). To examine the aggregation properties of the Rbfox CTD, we purified His-tagged recombinant proteins containing the wild type CTD or its mutant with ten tyrosines changed to serines (CTD-YS), each fused to a SNAP tag (Figure S1D). The SNAP-CTD fusion eluted largely in the void volume from a size exclusion column, with some unaggregated monomer. In contrast, nearly all of the CTD-YS mutant eluted as monomeric protein, indicating that it is less prone to aggregation (Figure S1B). We also made equivalent fusions with only the C2 fragment and its YS mutant. The SNAP-C2 fusion presented elution peaks in the void, as a multimer of about 150 kDa, and as monomer (Figure S1B). For the SNAP-C2-YS mutant, the void volume peak was reduced and the multimer eliminated, again indicating reduced aggregation. The recombinant CTD protein from the void volume peak was also analyzed on glycerol gradients. This E. coli purified protein sedimented as high molecular weight material starting at ~55S and extending to larger aggregates. In contrast, its YS mutant protein sedimented as an apparent monomer at the top of the glycerol gradient (Figure S1C).

The aggregation of the wild type and mutant fusion proteins was examined in a fluorescent phase separation assay previously applied to FUS and other proteins (Lin et al., 2015; Molliex et al., 2015; Patel et al., 2015). The SNAP-tagged wild type CTD and CTD-YS were fluorescently labeled with SNAP-surface 649, spiked into solutions of unlabeled protein, and monitored by fluorescence microscopy (Figure 3A). The labeled solutions remained monophasic and clear at room temperature in 150 mM NaCl. However, when the NaCl concentration was reduced to 37.5 mM, the CTD protein formed fluorescent fibrous structures after 21 hours. With longer incubation (48 hours) less concentrated solutions of

the CTD protein (6 μM instead of 12 μM) also formed aggregates. In contrast, the CTD-YS mutant remained in solution for days under the same conditions. The aggregates formed by the Rbfox CTD have a more irregular, fibrous appearance than the round liquid droplets reported with the FUS protein (Lin et al., 2015).

Fluorescent aggregates were only observed at salt concentrations lower than the 150 mM used in purification. It is possible that the soluble aggregates eluting in the void from the size exclusion column may seed the larger visible structures forming in low salt. To compare the aggregation seen by gel filtration with that seen by fluorescence microscopy, we also examined the monomeric fractions of the C2 fragment and its YS mutant (C2-YS; Figure S1B). We found that C2 but not C2-YS formed aggregates visible by microscopy in low salt (Figure 3B). Thus, even the apparent monomers isolated by gel filtration could form the larger aggregates observed by microscopy. These structures formed by the C2 protein were stained with Thioflavin T, a dye with high affinity for amyloid (Khurana et al., 2005), possibly indicating an amyloid-like assembly (Figure S1F).

We also tested if the crowding reagent polyethylene glycol (PEG) promoted the aggregation of SNAP-C2 proteins at low concentration. Adding 10% PEG8000 to solutions containing 0.5–1 μM protein caused SNAP-C2 to form round fluorescent concentrations even in 150 mM NaCl. An equivalent solution of SNAP-C2-YS remained clear (Figure S1E). SNAP-surface 549 labeled C2 or C2-YS were also incubated with C2 or C2-YS fused to monomeric EGFP (mEGFP). mEGFP-C2 was found to label the SNAP-surface 549 labeled C2 aggregates as well as form aggregates on its own (Figure 3C). The mEGFP-C2-YS protein did not label C2 aggregates indicating that the tyrosines are required for homotypic interactions of the C2 regions. Although they exhibit a rounder morphology than the aggregates seen in low salt, the C2 assemblies observed in PEG were not as spherical as the droplets observed for FUS and other proteins (Lin et al., 2015). It is not clear if these C2 assemblies are true liquid droplets.

In other assays, we compared the C2 and C2-YS polypeptides for their ability to form hydrogels and fibers. After incubation at room temperature for several days, concentrated mEGFP-C2 (~ 80 mg/ml) formed a hydrogel material, whereas the mEGFP-C2-YS did not (Figure S1G). The hydrogel formed by mEGFP-C2 and the ungelled mEGFP-C2-YS were resuspended in buffer, applied to EM grids and stained. The C2 protein but not C2-YS formed prominent fibers observable by transmission electron microscopy (Figure S1H). Together, these data demonstrate that the repetitive tyrosine residues mediate the self-assembly of the Rbfox proteins into higher order structures. These structures have similarities to the amyloid-like aggregates observed for FUS, but appear to form less efficiently from soluble protein, perhaps due to the less regular repeat structure of the tyrosine sequences.

Rbfox proteins exhibit a speckled pattern of nuclear staining with an uneven concentration distribution typical for splicing factors ((Dent et al., 2010; Huang et al., 2012; Yang et al., 2008) and data not shown). Since the Rbfox CTD mediated its self-assembly *in vitro*, we examined the effect of the tyrosine residues on higher-order Rbfox interactions within cells. Wild type protein (WT), the ten-tyrosine-to-serine mutant (10Y), and the ΔCTD mutant

were fused to mEGFP, stably expressed as inducible genes in HEK293 cells, and examined by confocal microscopy (Figure 3D and Figure S2AB). Wild type Rbfox1 exhibited the expected speckled or granular pattern of fluorescence with uneven distribution in the nucleus and exclusion from the nucleoli. This was unlike mEGFP alone which concentrated in the nucleoli. Interestingly, the Rbfox1 10Y and ΔCTD mutants presented a diffuse localization pattern, more evenly distributed than wild type protein in the nucleoplasm, and were also found in the nucleoli (Figure 3D).

To quantify the differences between the granular staining of wild type Rbfox1 and the more diffuse localization of the mutant proteins, we measured individual pixel intensities across the DAPI-stained nuclear area, while excluding nucleoli (Polling et al., 2015). For each cell, we determined the mean pixel fluorescence and standard deviation to assess the variation in local protein concentration (Figure S2C and Table S1). We found that the distribution of WT protein exhibited significantly higher granularity than the 10Y protein (p-value = 0.00263), with much greater variation in pixel intensity. These data indicate that, as seen *in vitro*, the repeated tyrosines in the CTD cause greater aggregation of Rbfox within the nucleoplasm (Figure 3E). The Rbfox tyrosine-rich domain did not produce the dense inclusions seen with the pathological aggregation of FUS, but instead was required to concentrate Rbfox in nuclear speckles.

The Rbfox tyrosine-rich domain is required for GCAUG-dependent exon activation

The homophilic assembly of Rbfox/LASR creates regions of higher and lower concentration of these proteins in the nucleus. This may alter the ability of Rbfox/LASR to be recruited to target RNAs. The CTD interactions could also mediate long-range contacts between protein complexes on the same RNA. To test the requirements for LASR interaction and higher order assembly in Rbfox mediated splicing, we used two Rbfox-regulated minigene reporters expressed *in vivo*: Dup-E33 and Dup-E9* (Tang et al., 2009). Dup-E33 contains CACNA1C exon 33, which has a downstream UGCAUG site required for Rbfox enhanced exon inclusion. Dup-E9* contains a modified CACNA1C exon 9*, which has an upstream UGCAUG site and is repressed by Rbfox (Figure 4AB). To eliminate effects from endogenous Rbfox protein, these reporters were transiently expressed in a Flp-In 293 Rbfox2$^{-/-}$ cell line generated by CRISPR/Cas9 mediated deletion of a portion of the Rbfox2 gene (Figure S3A; (Damianov et al., 2016)). E33 was largely skipped in the Rbfox2$^{-/-}$ cells, but its splicing was strongly stimulated by transiently expressed wild type Rbfox1. Conversely, E9* was spliced into the DUP-E9* mRNA in the Rbfox2$^{-/-}$ cells and this splicing was strongly repressed by Rbfox1. In contrast, the ΔCTD mutant of Rbfox1 neither activated E33 nor repressed E9* (Figure 4B). Note that the ΔCTD protein carries the SV40 T antigen NLS to replace C-terminal NLS of Rbfox1 and is localized in the nucleus (Figure 1B and 3D). Thus, the CTD is required for both splicing activation and splicing repression by Rbfox1.

We further examined splicing of the reporter transcripts in cells expressing a series of tyrosine mutant Rbfox proteins. Interestingly, splicing repression and splicing activation showed different responses to these mutations. Mutation of increasing numbers of tyrosines to serines progressively decreased the activation of E33 by Rbfox1. The proteins missing 10

or more tyrosines were only slightly more active than the F126A mutant (FA) that has lost RNA binding (Auweter et al., 2006; Figure 1E and 4D). In contrast, E9* splicing was only minimally affected by the tyrosine mutations; the protein missing 13 tyrosines was still much more active than FA in repressing E9* (Figure 1E and 4E). The activation of exon 33 splicing apparently requires the higher-order assembly of the Rbfox1/LASR complex, but repression of exon 9* does not.

Since the CTD is sufficient both to bind LASR and form higher-order complexes, and its loss eliminates splicing regulation by Rbfox, it is possible that the RBD serves to simply recruit the CTD to the target RNA. To examine whether the CTD is sufficient for Rbfox-dependent splicing regulation, we performed tethering experiments. We replaced the UGCAUG elements in DUP-E33 and DUP-E9* with the MS2 stem-loop structure that is bound by the MS2 phage Coat Protein (MCP) (Figure 4G). We fused the CTD and its CTD-YS mutant to MCP (Figure 4H). The reporters carrying the MS2 binding sites were coexpressed in cells with the MCP fusions and assayed for splicing (Figure 4I). We found that MCP-CTD activated E33 splicing but MCP-CTD-YS did not. In contrast, neither protein could repress E9* from the upstream MS2 stem-loop (Figure 4I and 4J). These results are consistent with a previous study showing an MS2 tethered Rbfox CTD could activate but not repress splicing (Sun et al., 2012). This work found that an MCP fusion containing both the Rbfox RBD and the CTD was active for splicing repression. In our system, adding the RBD conferred a slight amount of exon 9* repression that just reached statistical significance (p-value = 0.0202 for MCP-ΔNTD versus MCP and 0.0326 for MCP-ΔNTD-YS versus MCP, respectively). Altogether these data indicate that splicing activation by a downstream binding site is mediated by the CTD. This CTD is presumably recruiting LASR, but will also engage in interactions mediated by the tyrosines. Since these experiments were carried out in an Rbfox2 null cell line that does not express endogenous Rbfox protein, the tethered CTD is not recruiting additional full length Rbfox to the MS2 site. Repression of exon 9* through its upstream binding site appears to be mechanistically distinct. Simply tethering the CTD and LASR in this position was not sufficient to alter splicing, while tethering the RBD plus the CTD induced some exon 9* repression and this repression did not require the tyrosines.

To assess whether the tyrosine mutations affect the binding of Rbfox to the pre-mRNA, we performed UV crosslinking and immunoprecipitation followed by RT-qPCR of the E33 and E9* reporter minigene pre-mRNAs (Figure S3BC). The level of Rbfox1-crosslinked E33 RNA was reduced by the ΔCTD mutation indicating an effect of LASR recruitment and/or higher-order assembly on Rbfox binding. Interestingly, the 10Y mutant also exhibited a strong reduction in binding, suggesting that higher-order assembly affects the recruitment of Rbfox to the E33 pre-mRNA. In contrast, while the ΔCTD mutation impaired the binding of Rbfox to the E9* pre-mRNA, the binding of the 10Y mutant to this transcript was similar to the WT protein (Figure S3B). These results indicate that the RBD alone is not sufficient for Rbfox binding to its targets. CTD interactions, presumably with LASR, also affect Rbfox recruitment to the RNA. Moreover, interactions with enhancing and repressing elements differ in their dependence on the tyrosine residues.

To assess the requirement for the tyrosine residues in the regulation of endogenous transcripts, we applied RASL-seq (RNA-mediated oligonucleotide annealing, selection and ligation with next-generation sequencing) (Li et al., 2012) to profile 5530 alternative splicing events. RNA was isolated from Rbfox2$^{-/-}$ cell lines stably expressing wild type Rbfox1 (WT), the ten-tyrosine-to-serine mutant (10Y), the RNA-binding-defective F126A mutant (FA), or no new protein (Ctrl) (three biological replicates each). For each alternative splicing event assayable in these cells, the ratio of included isoform to excluded isoform (In/Ex ratio) was measured, and these ratios were compared across all cell lines and replicates. Exons exhibiting greater than a 1.5-fold change in In/Ex ratio between WT Rbfox1 expressing cells and the control cells ($p<0.05$), and less than a 1.5-fold change between FA cells and the control cells were defined as Rbfox1 regulated. These criteria identify 206 Rbfox1-targeted cassette exons (Figure 5A, Table S2 and S3).

The In/Ex ratios for the Rbfox1 regulated exon set measured across all the samples were subjected to unsupervised hierarchical clustering. As expected, replicates of cells expressing the same protein were most similar and the values for the FA cells were most similar to the control (Figure 5A). The cells expressing WT Rbfox1 were most different from the other cells. The cells expressing the 10Y protein showed the most variability across replicates. Looking at individual exons across the different cell lines, the exons clustered into three groups with distinct splicing behavior. The 29 exons in Group 1 were repressed by Rbfox1, while the 49 exons in Group 2 and the 128 exons in Group 3 were activated by Rbfox1 (Figure 5A, Table S3). The behavior of individual exons in each group was confirmed by RT-PCR (Figure S4AB, Table S5). As seen for DUP-E9*, the Group 1 exons repressed by wild type Rbfox1 were also largely repressed by the 10Y mutant protein. For exons activated by Rbfox1, those in Group 3 were similar to DUP-E33 and lost regulation with the 10Y mutant (Figure 5A). With some variation between replicates, exons in Group 2 continued to be at least partially activated by 10Y, and some were equally affected by the WT and 10Y proteins (Figure 5A). For exons in Group 2, the median fold change of In/Ex ratio between WT to 10Y was close to 1, while for Group 3 there was nearly a 2-fold change of In/Ex ratio between WT and 10Y (Figure 5B). Like Group 2, most Group 1 exons repressed by Rbfox showed only small average changes in In/Ex ratio between WT and 10Y. However, there was some variation between replicate samples and this group was the smallest. It is possible that if more exons were assayed, some repressed exons would also require the tyrosine residues. Overall and as seen with the reporter genes, splicing repression and splicing activation showed different dependencies on the tyrosine residues of the CTD (Figure 4DE, 5 and Figure S4B). A substantial subset of exons activated by Rbfox required these residues and presumably the higher-order assembly of the Rbfox/LASR complex for splicing regulation.

To confirm whether exon repression and activation followed the previously described rules for the position of Rbfox binding, we mapped the positions of Rbfox binding sites for all the exons. For each group, we plotted the number of GCAUG elements in 50 nt bins across the 300 nt intervals upstream and downstream of each exon (Figure S4C). As predicted, Group 1 exons repressed by Rbfox were enriched for GCAUG elements upstream of the exon. The Group 2 and 3 exons activated by Rbfox showed peaks of GCAUG sites in the downstream intron. The GCAUG peak for Group 2 exons was closer to the activated exon than in Group 3 and these exons had a secondary peak upstream of the exons (Figure S4C). We also

examined the distributions of binding motifs for the LASR components hnRNP H, hnRNP M, hnRNP C (as defined in Damianov et al., 2016). The hnRNP H motifs adjacent to Group 1 and 2 exons showed enrichment peaks that roughly aligned with the GCAUG peaks. For the Group 3 exons, two peaks of downstream hnRNP H motifs were found to flank the GCAUG peak. Group 3 exons also exhibited a broad peak of hnRNP C motifs upstream. Enrichments of hnRNP C motifs adjacent to Group 1 and 2 exons, and of hnRNP M motifs were more difficult to judge with these small exon sets. It will be interesting to examine larger numbers of exons to develop clearer statistical differences in binding site placement for exons exhibiting different regulatory behaviors.

We previously found that binding motifs for hnRNP M and C were enriched in sequences adjacent to sites of Rbfox crosslinking in brain (Damianov et al., 2016). HnRNP H motifs were not enriched adjacent to these sites in brain. The adjacent peaks of hnRNP H and Rbfox motifs for exons regulated in HEK293 cells indicated that Rbfox recruitment in these cells may differ from brain. To look more closely at the Rbfox sites for these exons, we characterized Rbfox2 eCLIP sites in K562 and HepG2 cells available from ENCODE. Rbfox2 eCLIP clusters found upstream of Group 1 exons and downstream of Group 2 and 3 exons were compiled and frequencies of all pentamer motifs were measured within intervals extending 40 nucleotides upstream and downstream of each crosslink site. These frequencies were compared to a background set of 81-nucleotide genomic intervals randomly chosen from the introns containing eCLIP clusters. Although not as strongly as in brain, the HEK293 regulated exons show binding motifs of hnRNP M and hnRNP C enriched in the sequences adjacent to Rbfox binding sites (Table S4 and Figure S4D). More strikingly, hnRNP H binding motifs were very significantly enriched in sequences encompassing the ENCODE Rbfox2 eCLIP clusters. After the Rbfox site itself, hnRNP H motifs were the most enriched elements adjacent to sites of Rbfox crosslinking for all three groups of HEK293 regulated exons. This LASR component may play a more prominent role in Rbfox regulation in HEK293 cells than in brain. The three exon groups exhibited differences in their distributions of enriched motifs.

DISCUSSION

Rbfox requires both interaction with LASR and higher-order assembly to regulate splicing

In recent work, we found that the nuclear Rbfox protein associated with unspliced RNA was nearly all bound with the LASR complex, and that Rbfox altered the splicing activity of LASR components (Damianov et al., 2016). We now show that the Rbfox1 CTD is both necessary and sufficient for binding LASR and is essential for both splicing activation and repression. Both an earlier study and our results found that artificial tethering of the CTD downstream of an exon by MS2 was sufficient to activate splicing (Sun et al., 2012). This Rbfox-MS2 fusion is presumably recruiting LASR to the RNA, indicating that the altered assembly of the spliceosome may be directed by contacts on LASR rather than Rbfox.

Interestingly, we found that Rbfox proteins carrying smaller mutations within the CTD still efficiently bound to LASR but were altered in their ability to regulate splicing. Mutation of ten tyrosines (10Y) eliminated splicing activation by Rbfox on many exons. This loss of activation was also observed when the CTD-YS mutant was recruited via MS2. In contrast,

exons normally repressed by Rbfox, as well as a subset of activated exons were still regulated by this 10Y mutant protein. Several previous observations indicate that splicing activation and splicing repression by Rbfox are mediated by different contacts on the protein. It has long been known that exon activation is usually mediated by a downstream binding site, whereas splicing repression commonly requires upstream Rbfox binding, a position effect seen with multiple other regulators (Fu and Ares, 2014; Witten and Ule, 2011). We previously found that an isoform of Rbfox missing most of the RBD acts as a dominant negative protein to block splicing activation by full length Rbfox. This same internally deleted protein did not affect Rbfox dependent splicing repression (Damianov and Black, 2010). The Green lab recently identified a subset of Rbfox2 target exons coregulated by 3' processing factors CPSF and SYMPK. The Rbfox bound to these exons may also be associated with LASR, or this may be a different regulatory complex. They further found that on an activated exon, Rbfox2 stimulated U1 snRNP binding, but on a repressed exon Rbfox2 inhibited U2AF binding (Misra et al., 2015). We have not made similar observations on our test exons, but these results all point to distinct Rbfox interactions in splicing activation and repression.

The Rbfox contacts with LASR are apparently distributed along the CTD, as two different fragments C2 and C3 could pull down all the LASR components. When only the C2 was present, the LASR interaction became dependent on the tyrosines. Thus, some tyrosines may contact LASR, but in the full domain other residues may maintain the interaction and make the tyrosines nonessential. Although it did not affect full-length Rbfox binding to LASR, the 10Y mutation prevented the higher-order assembly of the Rbfox/LASR complex, and reduced splicing of many exons. It is possible that to be activated for splicing, these exons require multiple Rbfox/LASR complexes whose binding is augmented by preassembling Rbfox/LASR units in a larger complex. This could result in bringing distant segments of RNA closer together, similar to the base-paired RNA bridges described as allowing distal Rbfox elements to regulate splicing (Lovci et al., 2013). Alternatively, the higher order assembly may serve to concentrate the regulatory factors within a localized subnuclear space. In a region of active RNA synthesis, the higher levels of protein would allow more rapid assembly onto a nascent RNA. This is in keeping with the finding that the tyrosine-rich domain causes the enrichment of the protein in nuclear speckles. The Rbfox2 CTD was also found to bind the Polycomb Repressive Complex 2 and to affect transcriptional changes in cardiomyocytes (Wei et al., 2016). We have not found PRC2 in Rbfox/LASR complexes. It is possible that the PRC2 interaction is with a different Rbfox2 isoform and reflective of a different subnuclear compartment.

Aggregation and fiber formation by a splicing regulatory complex

Recent work has shown that the LC sequences in RNA binding proteins exhibit a variety of aggregation behaviors that allow their concentration into subcellular structures (Bergeron-Sandoval et al., 2016; Courchaine et al., 2016; Lin et al., 2015; Schwartz et al., 2013). In the cytoplasm, self-assembly drives a liquid-liquid phase separation to form cytoplasmic stress granules and transport granules (Jain et al., 2016). Similar phase transitions in the nucleus are thought to concentrate factors in the nucleolus and the Cajal body (Brangwynne, 2013;

Courchaine et al., 2016; Feric et al., 2016; Strzelecka et al., 2010), but their role in mRNA maturation is not clear.

LC sequences in proteins such as FUS also undergo a pathological aggregation into the insoluble amyloid-like fibrils and intracellular inclusions seen in ALS and other neurodegenerative diseases (Kim et al., 2013; Li et al., 2013). The relationship between the reversible aggregation mediating formation of non-membranous organelles and the irreversible aggregation into pathological inclusions is a subject of great interest. The aggregation of the Rbfox CTD shows both similarities and differences with FUS. At low salt, recombinant Rbfox forms small fluorescent foci similar to FUS, hnRNP A1 and other proteins (Lin et al., 2015). Rather than the spherical droplets seen with stress granule proteins, the Rbfox aggregates are irregular, and are moderately stained with Thioflavin T. At high protein concentrations, solutions of Rbfox form hydrogels consisting of fibrils similar to those described for FUS (Kato et al., 2012). Although all of these aggregation properties are dependent on the tyrosine residues, it is not clear whether the observed Rbfox fibers are composed of the stacked cross-beta structures seen with FUS. We hypothesize that the CTD assembles into a variety of multimeric forms. Complexes such as the 55S Rbfox/LASR and the multimers of purified proteins observed by gel filtration are smaller than aggregates seen as phase separated foci. Still more extensive assemblies of the CTD must comprise the hydrogel. It will be very interesting to gain structural insight into the nature of these Rbfox assemblies.

The functions of the diverse LC sequences found in splicing factors, including the many found in LASR components, are not known. A portion of the LASR complex sediments at 55S in the absence of Rbfox and this could result from LASR interactions with another protein or of LASR with itself. Across the many proteins regulating splicing, there will likely be a wide spectrum of self-assembly interactions. Most splicing regulators are seen to concentrate in nuclear speckles. These structures are not spherical but seem to fill the space adjacent to active chromatin (Sleeman and Trinkle-Mulcahy, 2014; Spector and Lamond, 2011). We find that mutation of the CTD tyrosines eliminates the enrichment of Rbfox in speckles and leads to a loss of nucleolar exclusion, perhaps indicating that the protein is no longer anchored to other nuclear structures. Since the assembly of Rbfox into higher order structures is required for proper regulation of splicing, it may serve to concentrate Rbfox/LASR in subnuclear locations close to its target genes. Our results thus tie the activity of a repetitive domain in splicing with both its ability to self-assemble and its localization properties in the nucleus.

STAR Methods

Contact for Reagent and Resource Sharing

Further information and requests for reagents can be fulfilled by Douglas L. Black (dougbmicrobio.ucla.edu).

Experimental Model and Subject Details

Cell lines—Flp-In T-REx 293 cells (Thermo Fisher Scientific, female) and Flp-In T-REx 293 Rbfox2$^{-/-}$ cells (female) were cultured in Dulbecco's Modified Eagle's Medium (Mediatech) containing L-glutamine and 10% FBS at 37 °C. All cell lines tested negative for mycoplasma contamination, but have not been further authenticated.

Method Details

Plasmid construction—The vectors pET28a-SNAP-Tev and pET28a-mEGFP-Tev were constructed by replacing the thrombin cleavage site of the original pET28a vector (Novagen) with SNAP (NEB) or mEGFP tag and a Tev cleavage site. The EGFP contains the A206K monomeric mutation. The full CTD or C2 fragment of Rbfox1 were cloned into the pET28a-SNAP-Tev or pET28a-mEGFP-Tev downstream of the Tev cleavage site for expression in *E. coli*. All constructs contain an N-terminal SNAP or mEGFP tag and a C-terminal 6xHis tag. Rbfox1 and its mutants were cloned into pcDNA5-FRT/TO vector with 3xHA-3xFLAG or mEGFP-FLAG or MCP-FLAG tag for expression in cells (Thermo Fisher Scientific). Tyrosine-to-serine mutations were introduced by QuickChange site-directed mutagenesis. The TGCATG sequence of DUP-E33 and DUP-E9* was replaced with the MS2 sequence: ACATGAGGATCACCCATGT to generate DUP-E33MS2 and DUP-E9*MS2. The sequences of all plasmids were confirmed by DNA sequencing.

Stable cell line generation—Flp-In T-REx 293 cells (Thermo Fisher Scientific) or Flp-In T-REx 293 Rbfox2$^{-/-}$ cells stably expressing 3xHA-3xFLAG-SV40NLS-Rbfox1 and its deletion mutants, 3xHA-3xFLAG-Rbfox1 and its tyrosine mutants, 3xHA-3xFLAG-Rbfox1 and Rbfox2 B40 or M43 variants, were generated using the Flp-In system (Thermo Fisher Scientific) according to the manufacturer's instructions. One copy of the SV40 NLS was added to all Rbfox1 deletion mutants, except the ΔCTD+C1 that has two copies of the SV40 NLS to ensure proper nuclear localization. Protein expression was induced with 500 ng/ml doxycycline for two days.

Protein complexes analysis—Subcellular fractionation from cells was performed as described (Damianov et al., 2016). Cell pellets were resuspended in nine volumes of ice-cold homogenization buffer (10 mM HEPES-KOH pH 7.9, 15 mM KCl, 1 mM EDTA, 1.8 M sucrose, 5% Glycerol, 0.15 mM Spermine, 0.5 mM Sperimidine) in a Wheaton Potter-Elvehjem style tissue grinder with a motor-driven pestle and homogenized on ice. The homogenate was transferred to an SW41Ti ultracentrifugation tube containing 3.5 ml of cushion buffer (10 mM HEPES-KOH pH 7.9, 15 mM KCl, 1 mM EDTA, 2.0 M sucrose, 10% Glycerol, 0.15 mM Spermine, 0.5 mM Sperimidine). The homogenate was overlaid onto the cushion and centrifuged at 28,100 rpm for 1 hr at 4 °C. The supernatant and cushion buffer were discarded and the pelleted nuclei were washed once in 10 ml Buffer A (10 mM HEPES-KOH pH 7.9, 15 mM KCl, 1 mM EDTA, 0.15 mM Spermine, 0.5 mM Sperimidine). The isolated nuclei were lysed for 10 min on ice in ten volumes of lysis buffer (20 mM HEPES-KOH pH 7.9, 150 mM NaCl, 1.5 mM $MgCl_2$, 0.5 mM DTT, 1× protease inhibitors, and 0.6% Triton X-100). Soluble and HMW fractions were separated by centrifugation at 14,000 rpm for 10 min at 4 °C. To extract nuclease- resistant protein complexes, the soluble fraction was removed and an equal volume of lysis buffer added to

the HMW pellet. Soluble and HMW fractions were incubated at room temperature on a rotator with 5 U/ml of Benzonase (Sigma-Aldrich) until the HMW pellet was resuspended and then cleared by centrifugation for 10 min at 14,000 rpm at 4 °C. HMW protein fractions were subjected to glycerol gradient ultracentrifugation. HMW protein fractions were loaded and centrifuged in an SW41Ti rotor (Beckman Coulter) at 32,000 rpm for 12 hrs at 4 °C. Gradients were fractionated from top to bottom into 24× 500 μl fractions. Proteins were analyzed by western blot.

FLAG-immunoprecipitation—Soluble or HMW fractions were incubated overnight at 4 °C with 10 μl packed FLAG M2 agarose beads (Sigma-Aldrich). The beads were washed four times with wash buffer (20 mM HEPES-KOH pH 7.9, 150 mM NaCl, and 0.05% Triton X-100). Flag-tagged proteins were eluted from beads over 1 hr at 4 °C in 50 μl of elution buffer (20 mM HEPES-KOH pH 7.9, 150 mM NaCl, and 150 μg/ml of 3xFLAG peptide). Proteins were analyzed by western blot or stained by SYPRO Ruby protein gel stain (Thermo Fisher Scientific).

UV crosslinking and immunoprecipitation—Monolayer Flp-In T-REx 293 Rbfox2$^{-/-}$ cells were irradiated with UV (254 nm) at 75 mJ/cm^2 on ice in a Stratalinker 1800 (Stratagene). Cells were harvested and lysed for 10 min on ice in ten volumes of lysis buffer (20 mM HEPES-KOH pH 7.9, 150 mM NaCl, 0.5 mM DTT, 1× protease inhibitors, and 0.6% Triton X-100) supplemented with 0.1% SDS. Whole-cell lysates were cleared by centrifugation at 14,000 rpm for 10 min at 4 °C. The cleared whole-cell lysates were diluted with 4 volumes of lysis buffer and incubated with FLAG M2 agarose beads (Sigma-Aldrich) overnight at 4 °C. The beads were washed five times with high-salt wash buffer (20 mM HEPES-KOH pH 7.9, 1M NaCl, 0.02% SDS) and two times with low-salt wash buffer (20 mM HEPES-KOH pH 7.9, 150 mM NaCl). The beads were treated with 20 U DNaseI (Roche) for 15 min at 37 °C, followed by proteinase K treatment at 37 °C for 15 min. Cros slinked RNA was extracted by phenol/chloroform and precipitated overnight. Amounts of crosslinked RNA were normalized to immunoprecipitated protein level and subjected to RT-qPCR.

RT-qPCR—RNA was reverse transcribed with random hexamers and Superscript III (Thermo Fisher Scientific). 1 μl of cDNA was used to run SYBR Green detection qPCR assays using SensiFAST SYBR Low-ROX kit (Bioline) on QuantStudio 6 Flex Real-Time PCR system (Thermo Fisher Scientific). Primer sequences are listed in Table S5.

Immunofluorescence and confocal imaging—Rbfox1 and its mutants fused to mEGFP were stably expressed in Flp-In T-REx 293 Rbfox2$^{-/-}$ cells. Cells were grown on coverslips pretreated with 0.1% poly-L-lysine hydrobromide (Sigma-Aldrich). Protein expression was induced by 100 ng/ml doxycycline for 24 hrs. Cells were fixed by 4% PFA for 10 min at room temperature and then washed three times with PBS. Cells were mounted in mounting media with DAPI (Thermo Fisher Scientific). Single-plane images were taken with a Zeiss LSM 7780 laser scanning confocal microscope using a 63× oil objective. GFP fluorescence intensity was capped at the saturation level using the Range Indicator in Zen Blue acquisition software. The same scanning parameters were used to image WT, 10Y and

ΔCTD conditions. A separate GFP fluorescence intensity cap was used in the SV40NLS (GFP control) condition.

Recombinant protein purification—Proteins were expressed in *E. coli* Rosetta2 (DE3). Bacteria were cultured in LB medium supplemented with 50 μg/ml Kanamycin and 34 μg/ml chloramphenicol at 37 °C and induced at OD600 of 0.6–0.8 with 0.5 mM IPTG at 25 °C for 4 hours. The harvested cells were resuspended in equilibration buffer (50 mM Tris-HCl pH 7.5, 500 mM NaCl) and lysed by sonication. After centrifugation, the soluble fractions of the cell lysates were loaded onto a HisTrap HP 5ml column (GE Healthcare) pre-equilibrated with the same buffer. The columns were washed with equilibration buffer containing 50 mM imidazole, and the target proteins were eluted with a linear gradient of equilibration buffer containing 50–500 mM imidazole. The proteins were further purified on Hiload Superdex 200 column (GE Healthcare) equilibrated in the buffer containing 50 mM Tris-HCl pH 7.5, and 150 mM NaCl. The purified proteins were concentrated with Amicon Ultra centrifugal filters (Millipore), and stored at −80 °C. The puri ties of purified proteins were confirmed by SDS-PAGE, and the concentrations were determined by absorbance at UV280.

Microscopic Aggregation Assays—Formation of microscopic aggregates was assayed for the formation of liquid droplets (Lin et al., 2015). Proteins were fluorescently labeled with SNAP-Surface 549 or SNAP-Surface 649 (NEB) at 37 °C for 30 min in dark. Puri fied bacterial proteins with 2% of the protein fluorescently labeled were diluted in 37.5 mM NaCl, 50 mM Tris pH 7.5, and 1mM DTT. Reactions were performed in 96-well glass bottom plates (MatTek) coated with 3% BSA for 15 minutes and sealed with PCR plate film (USA scientific) to minimize evaporation. Images were acquired on an LSM 510 Meta Confocal Microscope (Zeiss) or an Eclipse TE2000 epifluorescence microscope (Nikon).

Hydrogel formation—Hydrogels of mEGFP-C2 were formed as described previously (Kwon et al., 2013). In brief, proteins were concentrated to ~ 80 mg/ml in gelation buffer (50 mM Tris pH 7.5, 150 mM NaCl, 1 mM DTT). 50 μl of the concentrated protein was placed in a silicon tube and kept at 4 °C for several days.

Transmission Electron Microscopy—The hydrogel protein solutions (5 μl) were resuspended in gelation buffer and loaded onto a glow-discharged TEM grid (Electron Microscopy Sciences, FCF400-Cu) and stained with 0.8% uranyl formate. TEM images were obtained at 120 kV on a T12 quick cryoEM and cryoET (FEI).

***In vivo* splicing assays—**DUP-E33 and DUP-E9* were described previously (Tang et al., 2009). For these experiments, exonic and downstream UGCAUG elements in the original DUP-E9* were mutated to generate the modified DUP-E9* with a single upstream UGCAUG. Transfections were performed with BioT transfection reagent (Bioland Scientific). For each well in a 6-well plate, cells were transfected with a mixture of 4 μg of protein expression plasmid, 200 ng of reporter plasmid and 1.5 μl BioT. 48 hours after transfection, RNA was extracted from cells using Trizol (Thermo Fisher Scientific), and reverse transcribed with random hexamers and Superscript III (Thermo Fisher Scientific). Spliced products from minigene reporters were amplified by PCR (22 cycles) and separated by denaturing urea-PAGE. Splice products from endogenous genes were amplified by PCR

(20–22 cycles) with addition of SYBR Green I dye (Bio-rad) in the reaction and resolved by native PAGE. The amplified splice products were detected by Typhoon 9410 imager (GE Healthcare) and quantified by ImageQuant™ TL. Primer sequences are listed in Table S5.

RASL-seq library construction and sequencing—RASL-seq was performed as described (Li et al., 2012) with some modifications. Total RNA from cells expressing Rbfox1 mutants were extracted with Trizol (Thermo Fisher Scientific) and treated with DNase I (Roche). RASL-seq oligonucleotides (a gift from Xiang-Dong Fu, UCSD) were annealed to 1 μg of total RNA, followed by selection by oligo-dT beads. Paired probes templated by polyA$^+$ RNA were ligated and then eluted. 5 μl of the eluted ligated oligos were used for 10 cycles of PCR amplification using primers F1: 5'-CCGAGATCTACACTCTTTCCCTACACGACGGCGACCACCGAGAT-3' and R1: 5'-GTGACTGGAGTTCAGACGTGTGCGCTGATGCTACGACCACAGG-3'. Half of the resulting PCR products were used in the second round of PCR amplification (10–15 cycles) using primers F2: 5'-AATGATACGGCGACCACCGAGATCTACACTCTTTCCCTACACG-3' and D701–D712 adapters (Illumina). The indexed PCR products were pooled and sequenced on a Miseq with a custom sequencing primer 5'-ACACTCTTTCCCTACACGACGGCGACCACCGAGAT-3' and a custom index sequencing primer 5'-TAGCATCAGCGCACACGTCTGAACTCCAGTCAC-3'.

Quantification and Statistical Analysis

Quantitative data are presented as mean ± SEM. All experiments were independently repeated at least three times. Statistical details of experiments and statistical significance can be found in the figure legends.

mEGFP pixel intensity quantification—The analysis of mEGFP pixel intensity in microscopic images of cells was performed as described previously with modifications (Polling et al., 2015). The nuclear areas excluding nucleoli were defined by DAPI signal using ImageJ 1.51j. The nucleus and nucleoli were traced using a thresholded image of the DAPI channel. Nucleolar areas were subtracted from the total nuclear area using the XOR function in the ROI (region of interest) manager. The final ROI was applied to the GFP channel and grey values were measured. The mean and standard deviation of mEGFP pixel intensity was measured for each cell using ImageJ. A homogenous protein distribution results in a low standard deviation of pixel intensity, while granularity results in higher standard deviation relative to the mean fluorescence. A two-sided P value was determined from an analysis of covariance test comparing the linear regression slopes from plots of the mean fluorescence against the standard deviation for approximately 60 individual cells.

RASL-seq analysis—Sequencing reads were mapped to the RASL-seq oligo pool sequences with Blat (Kent, 2002), allowing for two mismatches. On average, 1.3 million reads were obtained for each sample. Splicing events were filtered for a minimum of 5 reads averaged across all samples. Ratios of the counts of long to short isoforms (In/Ex ratio) were calculated. The significantly changed events were identified by average fold change and t-test ($p < 0.05$, comparing wild type Rbfox1 to control). Heat maps were generated by

hierarchical clustering using R. No statistical methods were used to predetermine the sample size for these experiments.

Motif enrichment analysis—Motif enrichment analysis was performed as described previously (Damianov et al., 2016). eCLIP clusters located at the upstream and downstream introns of Rbfox-regulated exons identified by RASL-seq were extracted from Rbfox2 eCLIP experiments in the ENCODE project database (GEO: GSE92030 and GSE92211). The binding regions, defined as including 40 nucleotides upstream and 40 nucleotides downstream of each crosslinking site, were analyzed for enrichment of nucleotide pentamers. To control for nucleotide frequency biases, pentamer frequencies in the binding regions were compared to the distribution of pentamer frequencies in a large set of 81-nucleotide genomic intervals randomly chosen from the introns containing eCLIP clusters.

Supplementary Material

Refer to Web version on PubMed Central for supplementary material.

Acknowledgments

We thank Xiang-Dong Fu and Jinsong Qiu (UCSD) for the RASL oligos and advice on RASL-seq; and Ben Blencowe and Serge Gueroussov for communicating unpublished results. This work was supported by the Howard Hughes Medical Institute and NIH grant R01 GM114463 (to D.L.B.); UCLA dissertation year fellowship and the China Scholarship Council (to Y.Y.); NIH F31 NS093923 (to C.K.V.); and the Broad Center for Stem Cell Research at UCLA.

References

Aguzzi A, Altmeyer M. Phase Separation: Linking Cellular Compartmentalization to Disease. Trends in cell biology. 2016; 26:547–558. [PubMed: 27051975]

Auweter SD, Fasan R, Reymond L, Underwood JG, Black DL, Pitsch S, Allain FH. Molecular basis of RNA recognition by the human alternative splicing factor Fox-1. The EMBO journal. 2006; 25:163–173. [PubMed: 16362037]

Bergeron-Sandoval LP, Safaee N, Michnick SW. Mechanisms and Consequences of Macromolecular Phase Separation. Cell. 2016; 165:1067–1079. [PubMed: 27203111]

Bill BR, Lowe JK, Dybuncio CT, Fogel BL. Orchestration of neurodevelopmental programs by RBFOX1: implications for autism spectrum disorder. International review of neurobiology. 2013; 113:251–267. [PubMed: 24290388]

Brangwynne CP. Phase transitions and size scaling of membrane-less organelles. J Cell Biol. 2013; 203:875–881. [PubMed: 24368804]

Calabretta S, Richard S. Emerging Roles of Disordered Sequences in RNA-Binding Proteins. Trends Biochem Sci. 2015; 40:662–672. [PubMed: 26481498]

Conboy JG. Developmental regulation of RNA processing by Rbfox proteins. Wiley interdisciplinary reviews RNA. 2017; 8

Conchillo-Sole O, de Groot NS, Aviles FX, Vendrell J, Daura X, Ventura S. AGGRESCAN: a server for the prediction and evaluation of "hot spots" of aggregation in polypeptides. Bmc Bioinformatics. 2007; 8

Courchaine EM, Lu A, Neugebauer KM. Droplet organelles? The EMBO journal. 2016; 35:1603–1612. [PubMed: 27357569]

Damianov A, Black DL. Autoregulation of Fox protein expression to produce dominant negative splicing factors. Rna. 2010; 16:405–416. [PubMed: 20042473]

Damianov A, Ying Y, Lin CH, Lee JA, Tran D, Vashisht AA, Bahrami-Samani E, Xing Y, Martin KC, Wohlschlegel JA, et al. Rbfox Proteins Regulate Splicing as Part of a Large Multiprotein Complex LASR. Cell. 2016; 165:606–619. [PubMed: 27104978]

Dent MA, Segura-Anaya E, Alva-Medina J, Aranda-Anzaldo A. NeuN/Fox-3 is an intrinsic component of the neuronal nuclear matrix. FEBS letters. 2010; 584:2767–2771. [PubMed: 20452351]

Eisenberg D, Jucker M. The Amyloid State of Proteins in Human Diseases. Cell. 2012; 148:1188–1203. [PubMed: 22424229]

Feric M, Vaidya N, Harmon TS, Mitrea DM, Zhu L, Richardson TM, Kriwacki RW, Pappu RV, Brangwynne CP. Coexisting Liquid Phases Underlie Nucleolar Subcompartments. Cell. 2016; 165:1686–1697. [PubMed: 27212236]

Fu XD, Ares M Jr. Context-dependent control of alternative splicing by RNA-binding proteins. Nat Rev Genet. 2014; 15:689–701. [PubMed: 25112293]

Gehman LT, Stoilov P, Maguire J, Damianov A, Lin CH, Shiue L, Ares M Jr, Mody I, Black DL. The splicing regulator Rbfox1 (A2BP1) controls neuronal excitation in the mammalian brain. Nature genetics. 2011; 43:706–711. [PubMed: 21623373]

Huang SC, Ou AC, Park J, Yu F, Yu B, Lee A, Yang G, Zhou A, Benz EJ Jr. RBFOX2 promotes protein 4.1R exon 16 selection via U1 snRNP recruitment. Molecular and cellular biology. 2012; 32:513–526. [PubMed: 22083953]

Jain S, Wheeler JR, Walters RW, Agrawal A, Barsic A, Parker R. ATPase-Modulated Stress Granules Contain a Diverse Proteome and Substructure. Cell. 2016; 164:487–498. [PubMed: 26777405]

Kato M, Han TW, Xie S, Shi K, Du X, Wu LC, Mirzaei H, Goldsmith EJ, Longgood J, Pei J, et al. Cell-free formation of RNA granules: low complexity sequence domains form dynamic fibers within hydrogels. Cell. 2012; 149:753–767. [PubMed: 22579281]

Kent WJ. BLAT--the BLAST-like alignment tool. Genome research. 2002; 12:656–664. [PubMed: 11932250]

Khurana R, Coleman C, Ionescu-Zanetti C, Carter SA, Krishna V, Grover RK, Roy R, Singh S. Mechanism of thioflavin T binding to amyloid fibrils. J Struct Biol. 2005; 151:229–238. [PubMed: 16125973]

Kim HJ, Kim NC, Wang YD, Scarborough EA, Moore J, Diaz Z, MacLea KS, Freibaum B, Li SQ, Molliex A, et al. Mutations in prion-like domains in hnRNPA2B1 and hnRNPA1 cause multisystem proteinopathy and ALS. Nature. 2013; 495:467–473. [PubMed: 23455423]

Kroschwald S, Maharana S, Mateju D, Malinovska L, Nuske E, Poser I, Richter D, Alberti S. Promiscuous interactions and protein disaggregases determine the material state of stress-inducible RNP granules. eLife. 2015; 4:e06807. [PubMed: 26238190]

Kwon I, Kato M, Xiang S, Wu L, Theodoropoulos P, Mirzaei H, Han T, Xie S, Corden JL, McKnight SL. Phosphorylation-regulated binding of RNA polymerase II to fibrous polymers of low-complexity domains. Cell. 2013; 155:1049–1060. [PubMed: 24267890]

Lagier-Tourenne C, Cleveland DW. Rethinking ALS: The FUS about TDP-43. Cell. 2009; 136:1001–1004. [PubMed: 19303844]

Lal D, Reinthaler EM, Altmuller J, Toliat MR, Thiele H, Nurnberg P, Lerche H, Hahn A, Moller RS, Muhle H, et al. RBFOX1 and RBFOX3 mutations in rolandic epilepsy. PloS one. 2013; 8:e73323. [PubMed: 24039908]

Lee JA, Damianov A, Lin CH, Fontes M, Parikshak NN, Anderson ES, Geschwind DH, Black DL, Martin KC. Cytoplasmic Rbfox1 Regulates the Expression of Synaptic and Autism-Related Genes. Neuron. 2016; 89:113–128. [PubMed: 26687839]

Lee JA, Tang ZZ, Black DL. An inducible change in Fox-1/A2BP1 splicing modulates the alternative splicing of downstream neuronal target exons. Genes & development. 2009; 23:2284–2293. [PubMed: 19762510]

Lee Y, Rio DC. Mechanisms and Regulation of Alternative Pre-mRNA Splicing. Annual review of biochemistry. 2015; 84:291–323.

Li, H., Qiu, J., Fu, XD. RASL-seq for massively parallel and quantitative analysis of gene expression. In: Frederick, M Ausubel, et al., editors. Current protocols in molecular biology. 2012. p. 11-19.Chapter 413

Li YR, King OD, Shorter J, Gitler AD. Stress granules as crucibles of ALS pathogenesis. J Cell Biol. 2013; 201:361–372. [PubMed: 23629963]

Lin Y, Protter DS, Rosen MK, Parker R. Formation and Maturation of Phase-Separated Liquid Droplets by RNA-Binding Proteins. Molecular cell. 2015; 60:208–219. [PubMed: 26412307]

Lovci MT, Ghanem D, Marr H, Arnold J, Gee S, Parra M, Liang TY, Stark TJ, Gehman LT, Hoon S, et al. Rbfox proteins regulate alternative mRNA splicing through evolutionarily conserved RNA bridges. Nature structural & molecular biology. 2013; 20:1434–1442.

Misra A, Ou J, Zhu LJ, Green MR. Global Promotion of Alternative Internal Exon Usage by mRNA 3' End Formation Factors. Molecular cell. 2015; 58:819–831. [PubMed: 25921069]

Molliex A, Temirov J, Lee J, Coughlin M, Kanagaraj AP, Kim HJ, Mittag T, Taylor JP. Phase Separation by Low Complexity Domains Promotes Stress Granule Assembly and Drives Pathological Fibrillization. Cell. 2015; 163:123–133. [PubMed: 26406374]

Murakami T, Qamar S, Lin JQ, Schierle GS, Rees E, Miyashita A, Costa AR, Dodd RB, Chan FT, Michel CH, et al. ALS/FTD Mutation-Induced Phase Transition of FUS Liquid Droplets and Reversible Hydrogels into Irreversible Hydrogels Impairs RNP Granule Function. Neuron. 2015; 88:678–690. [PubMed: 26526393]

Nakahata S, Kawamoto S. Tissue-dependent isoforms of mammalian Fox-1 homologs are associated with tissue-specific splicing activities. Nucleic acids research. 2005; 33:2078–2089. [PubMed: 15824060]

Nott TJ, Petsalaki E, Farber P, Jervis D, Fussner E, Plochowietz A, Craggs TD, Bazett-Jones DP, Pawson T, Forman-Kay JD, et al. Phase transition of a disordered nuage protein generates environmentally responsive membraneless organelles. Molecular cell. 2015; 57:936–947. [PubMed: 25747659]

Parikshak NN, Swarup V, Belgard TG, Irimia M, Ramaswami G, Gandal MJ, Hartl C, Leppa V, Ubieta LD, Huang J, et al. Genome-wide changes in lncRNA, splicing, and regional gene expression patterns in autism. Nature. 2016; 540:423–427. [PubMed: 27919067]

Patel A, Lee HO, Jawerth L, Maharana S, Jahnel M, Hein MY, Stoynov S, Mahamid J, Saha S, Franzmann TM, et al. A Liquid-to-Solid Phase Transition of the ALS Protein FUS Accelerated by Disease Mutation. Cell. 2015; 162:1066–1077. [PubMed: 26317470]

Polling S, Ormsby AR, Wood RJ, Lee K, Shoubridge C, Hughes JN, Thomas PQ, Griffin MDW, Hill AF, Bowden Q, et al. Polyalanine expansions drive a shift into alpha-helical clusters without amyloid-fibril formation. Nature structural & molecular biology. 2015; 22:1008–1015.

Schwartz JC, Cech TR, Parker RR. Biochemical Properties and Biological Functions of FET Proteins. Annual review of biochemistry. 2015; 84:355–379.

Schwartz JC, Wang X, Podell ER, Cech TR. RNA seeds higher-order assembly of FUS protein. Cell reports. 2013; 5:918–925. [PubMed: 24268778]

Sharma S, Falick AM, Black DL. Polypyrimidine tract binding protein blocks the 5' splice site-dependent assembly of U2AF and the prespliceosomal E complex. Molecular cell. 2005; 19:485–496. [PubMed: 16109373]

Singh G, Pratt G, Yeo GW, Moore MJ. The Clothes Make the mRNA: Past and Present Trends in mRNP Fashion. Annual Review of Biochemistry. 2015; 84:325–354. 84.

Sleeman JE, Trinkle-Mulcahy L. Nuclear bodies: new insights into assembly/dynamics and disease relevance. Curr Opin Cell Biol. 2014; 28:76–83. [PubMed: 24704702]

Spector DL, Lamond AI. Nuclear Speckles. Csh Perspect Biol. 2011; 3

Strzelecka M, Trowitzsch S, Weber G, Luhrmann R, Oates AC, Neugebauer KM. Coilin-dependent snRNP assembly is essential for zebrafish embryogenesis. Nature structural & molecular biology. 2010; 17:403–409.

Sun S, Zhang Z, Fregoso O, Krainer AR. Mechanisms of activation and repression by the alternative splicing factors RBFOX1/2. Rna. 2012; 18:274–283. [PubMed: 22184459]

Tang ZZ, Zheng S, Nikolic J, Black DL. Developmental control of CaV1.2 L-type calcium channel splicing by Fox proteins. Molecular and cellular biology. 2009; 29:4757–4765. [PubMed: 19564422]

Voineagu I, Wang X, Johnston P, Lowe JK, Tian Y, Horvath S, Mill J, Cantor RM, Blencowe BJ, Geschwind DH. Transcriptomic analysis of autistic brain reveals convergent molecular pathology. Nature. 2011; 474:380–384. [PubMed: 21614001]

Wallace EW, Kear-Scott JL, Pilipenko EV, Schwartz MH, Laskowski PR, Rojek AE, Katanski CD, Riback JA, Dion MF, Franks AM, et al. Reversible, Specific, Active Aggregates of Endogenous Proteins Assemble upon Heat Stress. Cell. 2015; 162:1286–1298. [PubMed: 26359986]

Wei CL, Xiao R, Chen L, Cui HW, Zhou Y, Xue YC, Hu J, Zhou B, Tsutsui T, Qiu JS, et al. RBFox2 Binds Nascent RNA to Globally Regulate Polycomb Complex 2 Targeting in Mammalian Genomes. Molecular cell. 2016; 62:875–889. [PubMed: 27211866]

Weyn-Vanhentenryck SM, Mele A, Yan Q, Sun S, Farny N, Zhang Z, Xue C, Herre M, Silver PA, Zhang MQ, et al. HITS-CLIP and integrative modeling define the Rbfox splicing-regulatory network linked to brain development and autism. Cell reports. 2014; 6:1139–1152. [PubMed: 24613350]

Witten JT, Ule J. Understanding splicing regulation through RNA splicing maps. Trends Genet. 2011; 27:89–97. [PubMed: 21232811]

Wootton JC, Federhen S. Analysis of compositionally biased regions in sequence databases. Method Enzymol. 1996; 266:554–571.

Yang G, Huang SC, Wu JY, Benz EJ Jr. Regulated Fox-2 isoform expression mediates protein 4.1R splicing during erythroid differentiation. Blood. 2008; 111:392–401. [PubMed: 17715393]

HIGHLIGHTS

- The Rbfox C-terminal domain is sufficient to recruit LASR and required for splicing.
- Higher order Rbfox/LASR assembly requires repetitive tyrosine residues in the CTD.
- Rbfox aggregation, speckled localization and splicing activation require tyrosines.
- Aggregation of RBPs plays a role in alternative splicing.

In Brief

Higher order protein assemblies shape alternative splicing

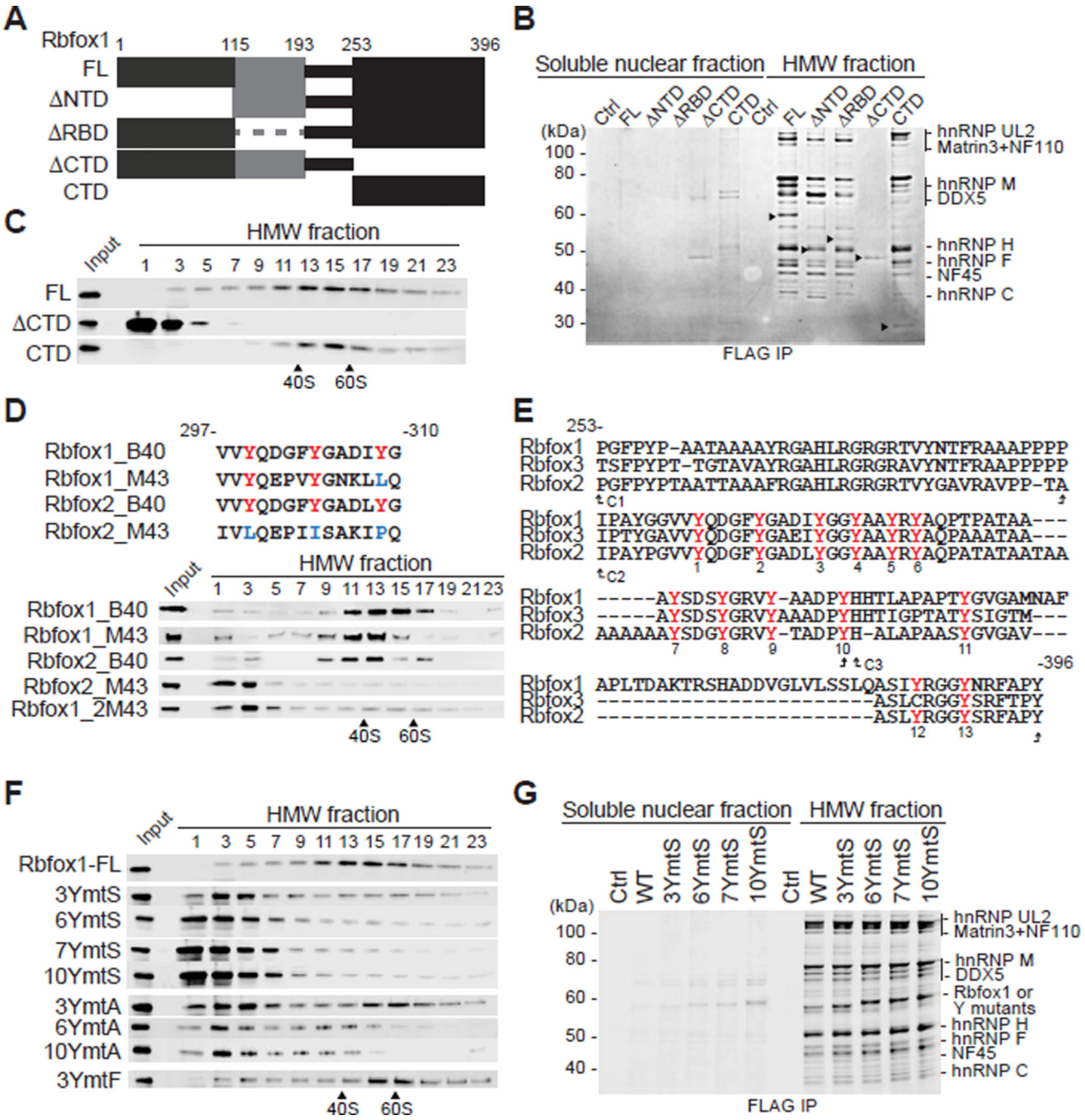

Figure 1. The Rbfox C-terminal domain (CTD) mediates both LASR binding and higher-order assembly

(A) Diagram of Rbfox1 domains and deletion mutants.

(B) Co-immunoprecipitation of LASR with Rbfox1 and mutants. Soluble and high molecular weight (HMW) nuclear fractions were prepared from Flp-In T-REx 293 cells stably expressing either full-length HA-FLAG-SV40NLS-Rbfox1 (FL) or a deletion mutant as diagrammed in (A). Anti-FLAG immunoprecipitates were eluted with FLAG peptide, separated on gels, and stained with SYPRO Ruby. Arrowheads indicate HA-FLAG-SV40NLS-Rbfox1 protein and its mutants. LASR subunits are indicated on the right.

(C) Sedimentation of Rbfox1 complexes in glycerol density gradients. HMW fractions of cells expressing Rbfox1 or an Rbfox1 fragment were loaded onto 10–50% glycerol density gradients. Gradient fractions from top to bottom run from left to right. Proteins from odd fractions were immunoblotted with anti-FLAG antibody. 40S and 60S markers are indicated below.

(D) Amino acid sequences encoded by exons B40 and M43 in Rbfox1 and Rbfox2 (top). Sedimentation of Rbfox1 and Rbfox2 splice variants in glycerol density gradients as in (C) (bottom).

(E) CTD sequence alignments for the nuclear B40 isoforms of Rbfox1, Rbfox2 and Rbfox3. Tyrosines examined by mutagenesis are shown in red. Sequences of C1, C2 and C3 fragments of CTD are indicated by arrows.

(F) Sedimentation of Rbfox1 tyrosine mutants in glycerol density gradients. Rbfox1 proteins containing increasing numbers of mutated tyrosines were separated as in (C). Three to ten tyrosine residues were mutated to serine, alanine or phenylalanine as indicated on the left.

(G) Immunoprecipitation of LASR with HA-FLAG-Rbfox1 containing tyrosine-to-serine mutations. Rbfox proteins and LASR subunits are indicated on the right.

See also Figure S1.

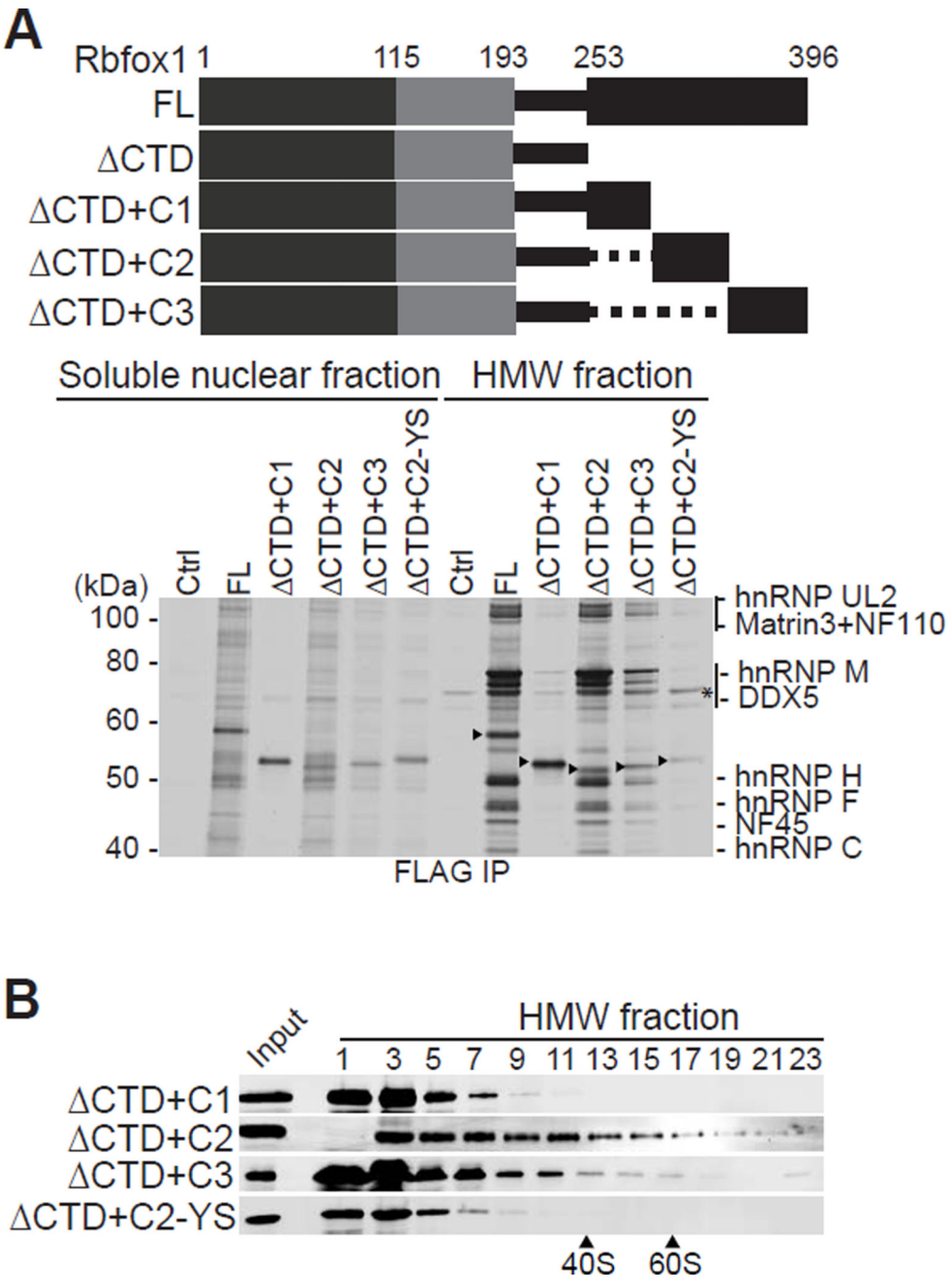

Figure 2. The Rbfox1 CTD makes multiple contacts with LASR

(A) Top: Diagram of Rbfox1 mutants containing different fragments of the CTD. Bottom: Immunoprecipitation of LASR with the Rbfox proteins. Arrowheads indicate the Rbfox protein and its mutants. LASR subunits are indicated on the right. The asterisk marks a non-specific band seen in the control IP.

(B) Sedimentation of Rbfox1 CTD mutants in glycerol density gradients.

See also Figure S1.

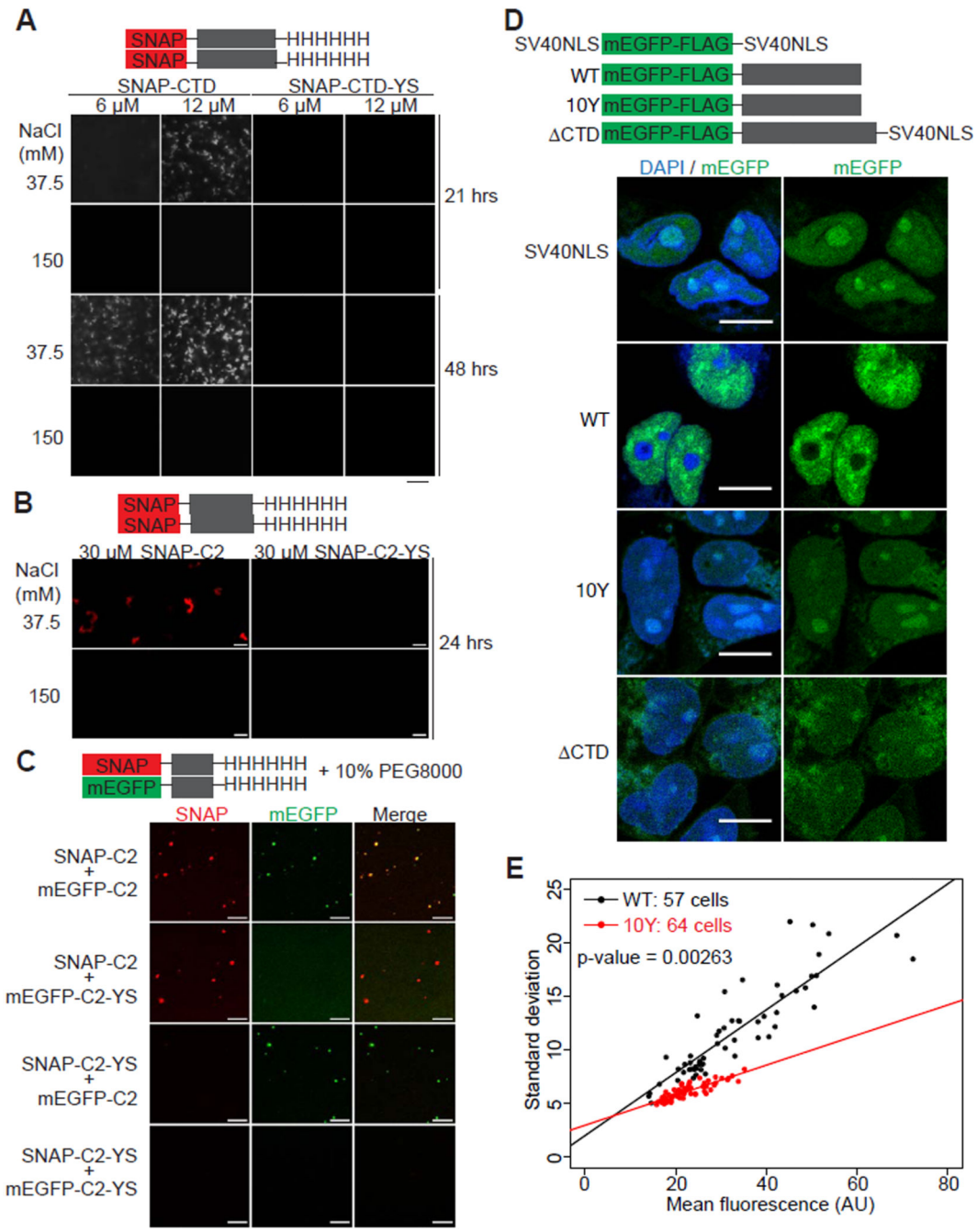

Figure 3. Aggregation of the Rbfox tyrosine-rich sequence *in vitro* and *in vivo*

(A) Top: Diagram of the SNAP-tagged Rbfox1 CTD with a C-terminal 6xHis tag and its ten-tyrosine-to-serine mutant (CTD-YS). Bottom: Epifluorescence microscopic images of aggregates formed by SNAP-CTD and SNAP-CTD-YS in 37.5 mM and 150 mM NaCl *in vitro*, at protein concentrations indicated on the top. Images were taken 21 hours and 48 hours after lowering the salt concentration. Scale bar: 5 μm.

(B) Top: Diagram of the SNAP-tagged Rbfox1 C2 fragment and its ten-tyrosine-to-serine mutant. Bottom: Confocal fluorescence microscopy images of structures formed by SNAP-

C2 and SNAP-C2-YS in 37.5 mM and 150 mM NaCl. Images were taken 24 hours after lowering the salt concentration. Scale bar: 5 μm.

(C) Top: Diagram of the SNAP and mEGFP-tagged Rbfox1 C2 fragment and its ten-tyrosine-to-serine mutant. Bottom: Confocal fluorescence microscopy images of the C2 fragment and C2-YS mutant. Solutions contained 0.5 μM of each protein and images were taken 24 hours after the addition of 10% PEG8000. Scale bar: 5 μm.

(D) Top: Diagram of the mEGFP-FLAG-tagged Rbfox1 protein and its mutants. Bottom: Confocal fluorescence microscopy images of cells stably expressing mEGFP-tagged Rbfox1 and its mutants. All images were taken with the same gain settings and other parameters, except the mEGFP signal of SV40NLS-ΔCTD where the gain was increased for better visualization. Additional images are provided in Figure S2A. Scale bar: 10 μm.

(E) Analysis of EGFP fluorescence in cells stably expressing mEGFP-FLAG-Rbfox1 (WT), and mEGFP-FLAG-Rbfox1 (10Y). The pixel intensity was measured across multiple nuclei, excluding the nucleoli, to obtain the mean and standard deviation of the fluorescent signal. Standard deviation from the mean was plotted against the mean fluorescence for 57 WT and 64 10Y mutant cells and fitted by linear regression. A P-value of 0.00263 was determined using a two-sided analysis of covariance test for comparison of WT versus 10Y slopes.

See also Figure S1, S2 and Table S1.

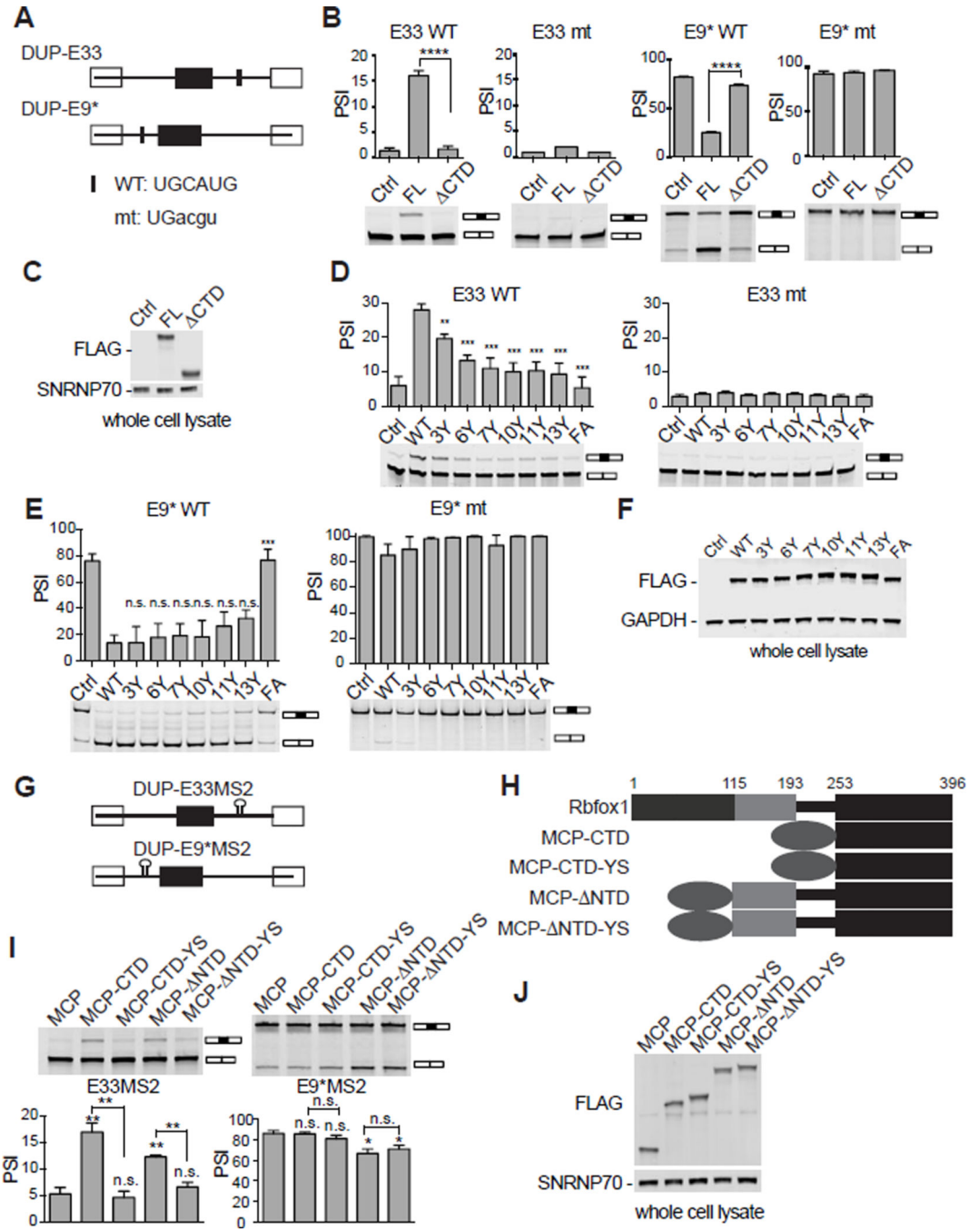

Figure 4. The CTD of Rbfox1 is required for splicing regulation

(A) Diagram of the DUP-E33 and DUP-E9* minigene reporters. The downstream and upstream UGCAUG sites are indicated. The sequence of the mutant element is shown below. (B) *In vivo* splicing assays of E33WT, E33mt, E9*WT, and E9*mt minigene reporters transiently expressed in cells carrying various Rbfox proteins. Gel electrophoresis of RT-PCR splicing assays is shown with spliced products indicated on the right. Bar graphs of PSI (percentage spliced in) calculated from three independent experiments are shown above each

gel. Error bars indicate the SEM. **** indicates $p < 0.0001$ by unpaired, one-tailed Student's t test between the Rbfox1 CTD deletion (ΔCTD) and full length Rbfox1 (FL).

(C) Immunoblot of Rbfox protein expression for the splicing assays in (B). Whole cell lysates were prepared from Flp-In T-REx 293 Rbfox2$^{-/-}$ cells transiently expressing full-length HA-FLAG-SV40NLS-Rbfox1 and its CTD deletion mutant and probed with antibodies to FLAG and SNRNP70.

(D) Assay of E33WT and E33mt exon splicing regulated by Rbfox tyrosine mutants. Gel electrophoresis of RT-PCR products from the DUP-E33WT and DUP-E33mt minigenes upon co-expression with the HA-FLAG-Rbfox1 tyrosine-to-serine mutants indicated on top. Spliced products are indicated on the right. Bar graphs of PSI calculated from three independent experiments are shown above each gel. Error bars indicate SEM. ** $p < 0.01$, *** $p < 0.001$, **** $p < 0.0001$ by unpaired, one-tailed Student's t test between each Rbfox1 tyrosine-to-serine mutant and wild type Rbfox1.

(E) Assay of DUP-E9*WT and DUP-E9*mt minigenes coexpressed with Rbfox tyrosine mutants. Products were separated and analyzed as in (D). Bar graphs showing PSI calculated from three independent experiments are shown above each gel. Error bars indicate the SEM. n.s., not significant by unpaired, one-tailed Student's t test between each Rbfox1 tyrosine-to-serine mutants and wild type Rbfox1.

(F) Immunoblot of Rbfox protein expression in the cells used for splicing assays in (D, E). Whole cell lysates were prepared from Flp-In T-REx 293 Rbfox2$^{-/-}$ cells transiently expressing HA-FLAG-Rbfox1 tyrosine mutants and probed with antibodies to FLAG and GAPDH.

(G) Diagram of the DUP-E33MS2 and DUP-E9*MS2 minigene reporters. The downstream and upstream MS2 stem-loop sites are indicated.

(H) Diagram of Rbfox1 mutants fused to MS2 coat protein (MCP). All proteins were FLAG-SV40NLS tagged.

(I) Splicing assays of the DUP-E33MS2 and DUP-E9*MS2 minigenes coexpressed with Rbfox1 mutants. Products were separated and analyzed as in (D). Bar graphs showing PSI calculated from three independent experiments are shown below each gel. Error bars indicate the SEM. Significance differences are indicated by * $p < 0.05$, ** $p < 0.01$, or n.s. (not significant) by unpaired, two-tailed Student's t test between each MCP-Rbfox1 fusion and MCP protein alone, or the pair indicated.

(J) Immunoblot of MCP-Rbfox1 fusion protein expression in cells used for splicing assays in (I). Whole cell lysates were prepared as in (F) and probed with antibodies to FLAG and SNRNP70.

See also Figure S3 and Table S5.

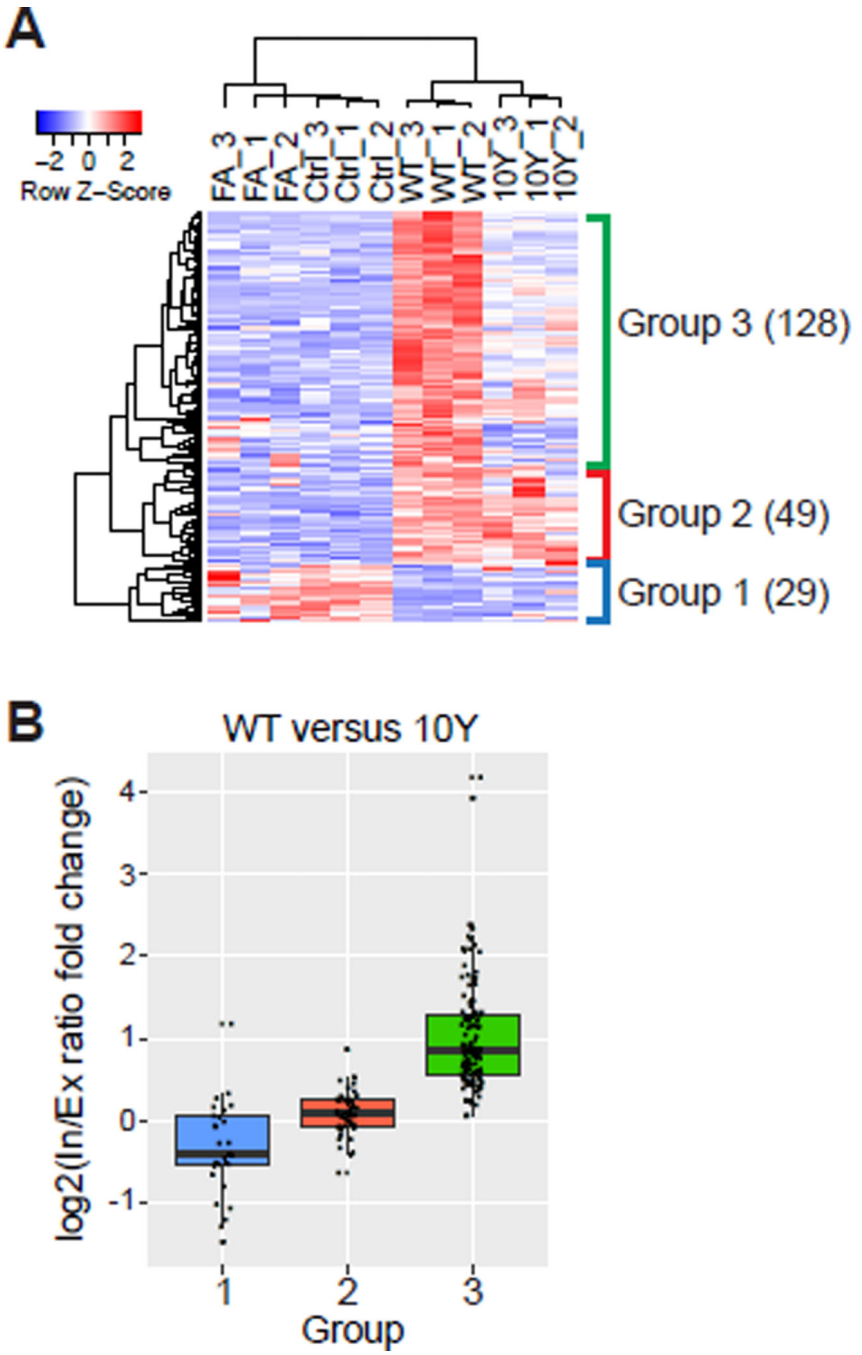

Figure 5. Higher-order assembly is required for Rbfox to activate a large set of target exons

(A) Heat map of exon In/Ex values for 206 cassette exons altered by Rbfox1 in Flp-In T-REx 293 Rbfox2$^{-/-}$ cells and measured by RASL-seq. Values were subjected to hierarchical clustering with rows corresponding to exons and columns to conditions of an expressed Rbfox protein and replicates. These conditions included the F126A mutant (FA), no protein (Ctrl), wild type Rbfox1 (WT), and the 10 tyrosine to serine mutant (10Y), each with three replicates. The clustering defined three exon groups exhibiting different responses to Rbfox1 and the 10Y mutant.

(B) Boxplots of the Log2 fold change between the WT In/Ex ratio and the 10Y In/Ex ratio plotted separately for Groups 1, 2 and 3. Each dot represents a cassette exon splicing event. The middle line indicates the median fold change in In/Ex ratio, with the box enclosing the quartiles of fold change values above and below the median.
See also Figure S4 and Table S2–S5.